Heat source-free water-floating carbon nanotube thermoelectric generators

Tomoyuki Chiba
Tokai University
Yuki Amma
Tokai University
Masayuki Takashiri (takashiri@tokai-u.jp)
Tokai University

Research Article

Keywords: thermoelectric generators, carbon nanotube, water environments

Posted Date: April 20th, 2021

DOI: https://doi.org/10.21203/rs.3.rs-428773/v1

Version of Record: A version of this preprint was published at Scientific Reports on July 19th, 2021. See the published version at https://doi.org/10.1038/s41598-021-94242-0.

Abstract

Thermoelectric generators (TEGs) produce electric power from environmental heat energy and are expected to play a key role in powering the Internet of things. However, they require a heat source to create a stable, irreversible temperature gradient. Overcoming these restrictions will allow the use of TEGs to proliferate. To this end, we propose heat source-free water-floating carbon nanotube (CNT) TEGs. Here, thermopower is generated by the temperature gradient in the CNT films in which water pumping via capillary action leads to water evaporation-induced cooling occurs in selected areas. Furthermore, the thermoelectric power increases when the films are exposed to sunlight and wind flow. These water-floating CNT TEGs demonstrate a pathway for developing wireless monitoring systems for water environments.

Main Text

Thermoelectric generators (TEGs) produce electricity from heat energy[1–3], with conventional TEGs connecting n- and p-type materials in series via metal electrodes[4–7]. Placing one end of a TEGs on a heat source induces a temperature gradient in the materials, with heat flowing in the direction along the temperature gradient. Additionally, electrons (n-type materials) and holes (p-type materials) move simultaneously in the direction of heat flow. Thus, current passes through the TEGs, generating electric power.

Recently, TEGs have been proposed as power supplies for the wireless sensors and wearable devices that constitute the Internet of things (IoT)[8–11]. These applications require TEGs that are small, lightweight, and mechanically flexible, without excessively high power caused by a large temperature gradient. Thin-film TEGs on a flexible substrate are the most promising candidate to satisfy these requirements[12–15]. To date, bismuth telluride-based alloys have proved a popular choice for thin-film TEGs owing to their impressive thermoelectric properties near room temperature[16–19]. Much research has been devoted to increasing the thermoelectric performance and optimizing the structure of TEGs[20–23]. However, current TEGs suffer from two major weaknesses. First, a heat source is required to create the temperature gradient in the TEGs. Second, heat flows vertically to the heat source and the direction cannot be controlled; therefore, p- and n-type materials are needed to produce electric power efficiently. Overcoming these weaknesses will allow the use of TEGs to expand unabated.

One promising TEG structure for surmounting these obstacles is water-floating carbon nanotube (CNT) TEGs (see Fig. 1). Carbon nanotubes are lightweight and possess both flexibility and mechanical strength[24–26]. In addition, single-wall carbon nanotubes (SWCNTs) with specific chirality exhibit relatively high thermoelectric properties near room temperature[27–30]. When a bundle of SWCNT films floats on water, the water passes through the gaps in the SWCNT bundle and reaches the surface via capillary action. When the water evaporates, heat is absorbed, and the surface temperature drops via evaporation-induced cooling. Moreover, this cooling effect can be enhanced by exposing the SWCNT films to sunlight

and wind flow. Designing the SWCNT films to have permeable and nonpermeable areas establishes a temperature gradient between these areas, enabling thermoelectric power to be generated via the Seebeck effect. This phenomenon indicates that TEGs can be fabricated using either p- or n-type materials alone. Typically, SWCNTs exhibit stable p-type properties[31]. In contrast, synthesizing air-stable n-type SWCNTs is extremely challenging[32–35]. Therefore, water-floating TEGs based on p-type SWCNT films are promising candidates to supply power to wireless environmental sensors used to measure the quality, quantity, and temperature of water. In addition, the TEGs have potential as wearable sensors where body sweat represents the water source.

Here, we report the fabrication and successful testing of water-floating TEGs using only p-type SWCNT films. The flexible substrate comprises square holes arranged in a staggered pattern, with each hole covered by an edge of a rectangular SWCNT film. The ends of adjacent SWCNT films are connected by metal electrodes. The temperature distribution in the TEGs was monitored as they floated on water. Thus, we verified that the heat flow can be controlled by evaporation-induced cooling and that the temperature gradient is stable. In addition, the thermoelectric power generated by the TEGs was measured in response to variations in water temperature, sunlight exposure, and wind exposure.

Fabrication and testing of water-floating SWCNT film TEGs

The process used to fabricate the water-floating SWCNT film TEGs is illustrated in Fig. 2a. Briefly, carbon nanotubes synthesized by the super-growth method (SG-CNTs) (ZEONANO SG101, ZEON Co.) were used as the starting material[36, 37]. Powdered SG-CNTs were dispersed in ethanol to prepare an SG-CNT dispersion solution with a concentration of 0.2 wt%. Next, an ultrasonic homogenizer (SONICS 85, AZONE Co.) was used to disperse the SG-CNT powder completely. The output power of the homogenizer was 60 W, and the dispersion time was 20 min. Because the vibrational energy during dispersion generates heat, the dispersion was conducted in a cold-water bath. The SWCNT films were prepared by a vacuum filtering method. A membrane filter (PTFE, 90 mm diameter: ADVANTEC) was placed in a filter holder in a suction bottle, and the dispersion solution was filtered by reducing the pressure in the suction bottle using a rotary pump to extract the material in the solution. A CNT-dispersed solution (40 mL) was released drop-by-drop onto the filter, and aspirated for 1 h to produce SWCNT films with a diameter of approximately 80 mm. After drying for 24 h in air, the SWCNT films were removed from the membrane filter. To assemble the TEGs, the SWCNT films were cut into four pieces, each measuring 45 mm in length and 15 mm in width. The substrate (80 mm × 60 mm, 125 μm thick) was a polyimide sheet (Kapton, DuPont) in which four rectangular holes (20 mm × 10 mm) were drilled in a staggered arrangement. The four sections of the SWCNT films were bonded to the substrate with silver paste such that adjacent films each covered half a hole in the polyimide. The SWCNT films were connected in series using thin copper wires. The cross-plane SEM image shows that the film was deposited almost uniformly, with a film thickness of approximately 50 μm (Fig. 2b). The surface SEM image shows the stacking of numerous winding SWCNT bundles with various diameters, including the presence of gaps between the bundles (Fig. 2c).

These gaps allow water to reach the surface via capillary action. The TEM image of the SWCNTs shows that their diameters measure several tens of nanometers, with the SWCNTs arranged in a one-dimensional linear structure (Fig. 2d).

We conducted our experiments assuming typical natural environment conditions. The SWCNT film TEGs were floated on a 450 mL volume of water at initial temperatures of approximately 20°C and 80°C. Wind was applied to the TEGs using a compact circulator (PCF-HD15-W, IRIS OHYAMA Inc.) while the wind speed (3.0 m/s) was measured by an anemometer (SP-82AT, Mother Tool Co.). The TEGs were irradiated using an artificial solar illuminator (XC-100, SERIC Ltd.) to simulate direct sunlight (approximate light intensity: 1000 W/m^2), with the intensity measured by a solar power meter (DT-1307, CEM Instruments). The temperature distribution in the TEGs was measured by a thermographic camera (Type F30W, Japan Avionics). The thermoelectric power was measured using a heat flow logger (LR8432, Hioki Co.).

Thermoelectric properties of SWCNTs and their films

The thermoelectric properties of the SWCNT films are presented in Table 1. The in-plane electrical conductivity, Seebeck coefficient, and power factor near 20°C are 88 S/cm, 55 μV/K, and 26.7 μW/(m·K^2), respectively. Additionally, the in- and cross-plane thermal diffusivities, D_{in} *and* D_{cross}, are 18.1 and 0.3 mm^2/s, respectively. The thermal conductivity can be determined from the thermal diffusivity (D), density (ρ), and specific heat (C_p) based on the equation $\kappa = D\rho C_p$[38]. The density of the SWCNT film was measured as 0.31 g/cm^3, while a specific heat of 0.96 J/(g·K) was referred from the literature[39]. As a result, the in- and cross-plane thermal conductivities were determined to be 5.4 and 9.0 × 10^{-2} W/(m·K), respectively, which are lower than those of SWCNT films reported previously owing to differences in the electrical conductivity due to different synthesis methods[40]. However, the lower thermal conductivities of the SWCNT films in this study facilitate effective temperature gradient generation in the films.

Performance of water-floating SWCNT film TEGs

The temperature distribution and performance of the water-floating SWCNT film TEGs in response to various environmental conditions are shown in Fig. 3. The ambient temperature in all experiments was approximately 20°C. A photograph of the experimental setup is provided in Fig. S1 (see Supplementary Material). For a water temperature of approximately 20°C, and in the absence of simulated sunlight and wind, the temperature gradients between the positions with and without substrate holes were invisible in the thermographic image (Fig. 3a). However, a stable thermoelectric power of approximately 120 μV was detected with four SWCNT films (Fig. 3b), indicating that an approximate temperature difference of 0.5 K occurred in each film based on the Seebeck coefficient of the SWCNT films (55 μV/K). As shown in Fig. S2 (see Supplementary Material), we verified that an almost constant value of thermoelectric power was

maintained when the TEGs floated on the water for 60 min, thereby demonstrating stable thermoelectric power generation without a heat source. The thermographic image in Fig. 3c shows that for an initial water temperature of 80°C (without simulated sunlight and wind), a clear temperature gradient is established between the positions with and without substrate holes. Furthermore, the ‘hot’ and ‘cold’ areas are located opposite each other on the adjacent films. This implies that the heat flow can be controlled by changing the position of holes in the substrate, and that only one type of (n-type or p-type) film is required to create the TEGs. The approximate temperature difference under these conditions was estimated to be 5 K, and the temperature gradient at edge of the holes is steep because the in-plane thermal conductivity of the SWCNT films (κ_{in} = 5.4 W/(m•K)) is not substantially higher than conventional thermal conductive materials ($\kappa \approx$ 400 W/(m•K) in copper). In addition, owing to the low thermal conductivity of the polyimide substate (κ = 0.16 W/(m•K)), heat is not transferred between adjacent films. These results demonstrate that the size of the films and the interval between them can be reduced to increase the power density of the TEGs as provided in Fig. S3 (see Supplementary Material). The thermoelectric power at a water temperature of 80°C was 950 μV. The thermoelectric power was observed to decrease with temperature, measuring 400 μV at a water temperature of 50°C (Fig. 3d). A temperature gradient was also observed when exposing the TEGs to simulated sunlight (1000 W/m^2) in a wind-free environment at a water temperature of 14°C (Fig. 3e). A stable thermoelectric power of approximately 450 μV was detected, indicating a temperature difference of 2 K in each film (Fig. 3f), representing a 3.7-fold increase in the thermoelectric power compared to the corresponding measurement without simulated sunlight and wind. This is attributed to the temperature of the SWCNT films at hole-free locations increasing owing to the film exhibiting extremely high light absorption, while the temperature of the films at the holes does not increase because of the cooling effect induced by water evaporation. As shown in Fig. S4 (see Supplementary Material), we verified that the humidity above the films at the holes was higher than that above the films at hole-free locations. The thermographic image in Fig. 3g, which corresponds to wind flow (3.0 m/s) without simulated sunlight at a water temperature of 18°C, shows a slight temperature gradient. In addition, a temperature difference between the SWCNT films and the water was also clearly observed. This is because the heat transfer from the water to the SWCNT films was limited by the relatively low cross-plane thermal conductivity of the SWCNT films (κ = 9.0 × 10^{-2} W/(m·K)). Based on the stable thermoelectric power of approximately 300 μV detected under these conditions, we can infer a temperature difference of 1.4 K in each film (Fig. 3h). Exposing the TEGs to a wind flow of 3 m/s increased the thermoelectric power by a factor of 2.5 relative to the wind and simulated sunlight-free measurement. It is considered that wind causes the concentration of water vapor near the film surface to decrease. As a result, water evaporation is promoted, which lowers the surface temperature. This suggests that the TEGs can generate the thermoelectric power at night. Our experiments demonstrate that water temperature, sunlight, and wind all affect the power generation of the TEGs. Therefore, we determined the combination of water temperature, sunlight exposure, and wind exposure required to optimize the power generation of the TEGs (Fig. 3g). Consequently, we realized a thermoelectric power of 1300 μV at a water temperature of 80°C, simulated sunlight of 1000 W/m^2, and wind speed of 3.0 m/s. Decreasing the water temperature while maintaining the other conditions resulted in the thermoelectric power decreasing, with a power of 800 μV recorded at a water temperature of 30°C

(Fig. 3h). Finally, we verified that the TEGs can generate the thermoelectric power in actual environmental conditions (natural sunlight and wind) as shown in Fig. S5 (see Supplementary Material).

Conclusion

In summary, we have conducted the first experimental study of thermoelectric power of water-floating SWCNT film TEGs. These results demonstrate that they can be enhanced by applying various environmental conditions. Nevertheless, for application as power sources for IoT sensors, the thermoelectric power of the TEGs requires further improvement: an input voltage of at least 20 mV is required to amplify the voltage via a booster circuit[41]. However, the thermoelectric power can be increased by optimizing the size of the SWCNT films and the holes in the substrate, as well as by increasing the number of smaller films. Therefore, this study provides a vital platform for further investigations to develop heat source-free power supplies for many wireless monitoring systems, such as water quality control. In addition, the TEGs can be used as wearable sensors that generate power using the evaporation of sweat from the skin surface. Once this system realizes, the health management and living environment in post-COVID-19 can be greatly improved.

Methods

The structural properties of the SWCNT films were analyzed using scanning electron microscopy (SEM: S-4800, Hitachi) and transmission electron microscopy (TEM: H7700, Hitachi). The in-plane electrical conductivity, σ, of the SWCNT films was measured to 20°C using a four-point probe method (Napson, RT-70V). The in-plane Seebeck coefficient, S, was also measured to 20°C using a custom-built instrument[42]. One end of a thin film was connected to a heat sink and the other to a heater. The Seebeck coefficient was determined as the ratio of the potential difference across the membrane to the temperature difference measured using two 0.1 mm-diameter K-type thermocouples pressed against the membrane. Then, the in-plane power factor, σS^2, was obtained from the measured electrical conductivity and Seebeck coefficient. The in-plane and cross-plane thermal diffusivities, D_{in} and D_{cross}, were measured using non-contact laser spot periodic heating radiation thermometry (TA33 thermowave analyzer, Bethel Co.).

References

1. DiSalvo, F. J. Thermoelectric cooling and power generation. *Science.* **285**, 703–706 (1999).
2. He, W. *et al.* Recent development and application of thermoelectric generator and cooler. *Appl. Energy.* **143**, 1–25 (2015).
3. Champier, D. Thermoelectric generators: A review of applications. *Energy Convers. Manage.* **140**, 167–181 (2017).

4. Matsubara, I. *et al.* Fabrication of an all-oxide thermoelectric power generator. *Appl. Phys. Lett.* **78**, 3627 (2001).
5. Snyder, G. J., Lim, J. R., Huang, C. K. & Fleurial, J. P. Thermoelectric microdevice fabricated by a MEMS-like electrochemical process. *Nat. Mater.* **2**, 528–531 (2003).
6. Takayama, K. & Takashiri, M. Multi-layered-stack thermoelectric generators using p-type Sb2Te3 and n-type Bi2Te3 thin films by radio-frequency magnetron sputtering. *Vacuum.* **144**, 164–171 (2017).
7. Kobayashi, A., Konagaya, R., Tanaka, S. & Takashiri, M. Optimized structure of tubular thermoelectric generators using n-type Bi2Te3 and p-type Sb2Te3 thin films on flexible substrate for energy harvesting. *Sens. Actuators, A.* **313**, 112199 (2020).
8. Paradiso, J. A. & Starner, T. Energy scavenging for mobile and wireless electronics. *IEEE Pervasive Comput.* **4**, 18–27 (2005).
9. Madan, D. *et al.* High-performance dispenser printed MA p-Type Bi0.5Sb1.5Te3 flexible thermoelectric generators for powering wireless sensor networks. *ACS Appl. Mater. Interfaces.* **5**, 11872–11876 (2013).
10. Bahk, J. H., Fang, H., Yazawa, K. & Shakouri, A. Flexible thermoelectric materials and device optimization for wearable energy harvesting. *J. Mater. Chem. C.* **3**, 10362 (2015).
11. Siddique, A. R. M., Rabari, R., Mahmud, S. & Heyst, B. V. Thermal energy harvesting from the human body using flexible thermoelectric generator (FTEG) fabricated by a dispenser printing technique. *Energy.* **115**, 1081–1091 (2016).
12. Yamamuro, H. *et al.* Combination of electrodeposition and transfer processes for flexible thin-film thermoelectric generators. *Coatings.* **8**, 2 (2018).
13. Fan, P. *et al.* Low-cost flexible thin film thermoelectric generator on zinc based thermoelectric materials. *Appl. Phys. Lett.* **106**, 073901 (2015).
14. Hamada, J., Yamamoto, K. & Takashiri, M. Fabrication and characterization of roll-type thin-film thermoelectric generators. *J. Phys. Conf. Ser.* **1052**, 012129 (2018).
15. Karthikeyan, V. *et al.* Wearable and flexible thin film thermoelectric module for multi-scale energy harvesting. *J. Power Sources.* **455**, 227983 (2020).
16. Venkatasubramanian, R., Siivola, E., Colpitts, T. & O'Quinn, B. Thin-film thermoelectric devices with high room-temperature figures of merit. *Nature.* **413**, 597–602 (2001).
17. Poudel, B. *et al.* High-thermoelectric performance of nanostructured bismuth antimony telluride bulk alloys. *Science.* **320**, 634–638 (2008).
18. Kashiwagi, M. *et al.* Enhanced figure of merit of a porous thin film of bismuth antimony telluride. *Appl. Phys. Lett.* **98**, 023114 (2011).
19. Kudo, S. *et al.* Determining the thermal conductivities of nanocrystalline bismuth telluride thin films using the differential 3ω method while accounting for thermal contact resistance. *J. Electron. Mater.* **44**, 2021–2025 (2015).

20. Morikawa, S., Inamoto, T. & Takashiri, M. Thermoelectric properties of nanocrystalline Sb2Te3 thin films: experimental evaluation and first-principles calculation, addressing effect of crystal grain size. *Nanotechnology.* **29**, 8 (2018).
21. Toan, N. V., Tuoi, T. T. & Ono, K. T. Thermoelectric generators for heat harvesting: From material synthesis to device fabrication. *Energy Convers. Manage.* **225**, 113442 (2020).
22. Kraemer, D. *et al.* High-performance flat-panel solar thermoelectric generators with high thermal concentration. *Nature Mater.* **10**, 532–538 (2011).
23. Courtney, H. *et al.* High-performance flexible bismuth telluride thin film from solution processed colloidal nanoplates. *Adv. Mater. Technol.* **5**, 2000600 (2020).
24. Iijima, S. & Ichihashi, T. Single-shell carbon nanotubes of 1-nm diameter. *Nature.* **363**, 603–605 (1993).
25. Yu, C., Choi, K., Yin, L. & Grunlan, J. C. Light-weight flexible carbon nanotube based organic composites with large thermoelectric power factors. *ACS Nano.* **5**, 7885–7892 (2011).
26. Maruyama, S., Kojima, R., Miyauchi, Y., Chiashi, S. & Kohno, M. Low-temperature synthesis of high-purity single-walled carbon nanotubes from alcohol. *Chem. Phys. Lett.* **360**, 229–234 (2002).
27. Small, J. P., Perez, K. M. & Kim, P. Modulation of thermoelectric power of individual carbon nanotubes. *Phys. Rev. Lett.* **91**, 256801 (2003).
28. Ichinose, Y. *et al.* Solving the Thermoelectric trade-off problem with metallic carbon nanotubes. *Nano Lett.* **19**, 7370–7376 (2019).
29. Ohnishi, M., Shiga, T. & Shiomi, J. Effects of defects on thermoelectric properties of carbon nanotubes. *Phys. Rev. B.* **95**, 155405 (2017).
30. Seki, Y. & Takashiri, M. Freestanding bilayers of drop-cast single-walled carbon nanotubes and electropolymerized poly(3,4-ethylenedioxythiophene) for thermoelectric energy harvesting. *Org. Electron.* **76**, 105478 (2020).
31. Blackburn, J. L. *et al.* Carbon-nanotube-based thermoelectric materials and devices. *Adv. Mater.* **30**, 1704386 (2018).
32. Nonoguchi, Y. *et al.* Systematic conversion of single walled carbon nanotubes into n-type thermoelectric materials by molecular dopants. *Sci. Rep.* **3**, 3344 (2013).
33. Seki, Y., Nagata, K. & Takashiri, M. Facile preparation of air-stable n-type thermoelectric single-wall carbon nanotube films with anionic surfactants. *Sci. Rep.* **10**, 8104 (2020).
34. Fukumaru, T. 1 & Fujigaya, T. & Nakashima1, N. Development of n-type cobaltocene-encapsulated carbon nanotubes with remarkable thermoelectric property. *Sci. Rep.* **5**, 7951 (2015).
35. Yonezawa, S., Chiba, T., Seki, Y. & Takashiri, M. Origin of n type properties in single wall carbon nanotube films with anionic surfactants investigated by experimental and theoretical analyses. *Sci. Rep.* **11**, 5758 (2021).
36. Hata, K. *et al.* Water-assisted highly efficient synthesis of impurity-free single-walled carbon nanotubes. *Science.* **306**, 1362–1364 (2004).

37. Chiba, T., Seki, Y. & Takashiri, M. Correlation between the air stability of n-type thermoelectric properties and defects in single-walled carbon nanotubes with anionic surfactants. *AIP Adv.* **11**, 015352 (2021).
38. Parker, W. J., Jenkins, R. J., Butler, C. P. & Abbott, G. L. Flash method of determining thermal diffusivity, heat capacity, and thermal conductivity. *J. Appl. Phys.* **32**, 1679–1684 (1961).
39. Oshima, K. *et al.* Enhancement of the electrical conductivity of defective carbon nanotube sheets for organic hybrid thermoelectrics by deposition of Pd nanoparticles. *Mater. Adv.* **1**, 2926–2936 (2020).
40. Nonoguchi, Y. *et al.* Simple salt-coordinated n-type nanocarbon materials stable in air. *Adv. Funct. Mater.* **26**, 3021–3028 (2016).
41. B *et al.* Printed, metallic thermoelectric generators integrated with pipe insulation for powering wireless sensors. *Appl. Energy.* **208**, 758–765 (2017).
42. Seki, Y., Takahashi, M. & Takashiri, M. Effects of different electrolytes and film thicknesses on structural and thermoelectric properties of electropolymerized poly(3,4-ethylenedioxythiophene) films. *RSC Adv.* **9**, 15957–15965 (2019).

Declarations

Acknowledgments: The authors acknowledge financial support from Zeon Corporation. We thank H. Uchida (Zeon Co.) for providing SG-SNT powders, Nishi (Ibaraki Univ.) for supporting the thermal diffusivity measurement, and S. Kuwahata (Tokai Univ.) for supporting the temperature measurement of TEGs.

Author contributions: T.C. and M.T. conceived the idea and designed the experiments. T.C., and M.T. wrote the main manuscript text. The experiments and data analysis were performed by T.C. and Y.A. with help from M.T. All authors discussed the results and commented on the manuscript.

Competing interests: Authors declare that they have no competing interests.

Data and materials availability: All data are available in the main text or the supplementary materials.

Tables

Table 1. Thermoelectric properties of SWCNT films.

SWCNT film	σ [S/cm]	S [μV/K]	PF [μW/(m K^2)]	D [mm^2/s]	κ [W/(m K)]
In-plane	88	55	26.7	18.1	5.4
Cross-plane	-	-	-	0.3	9.0×10^{-2}

Figures

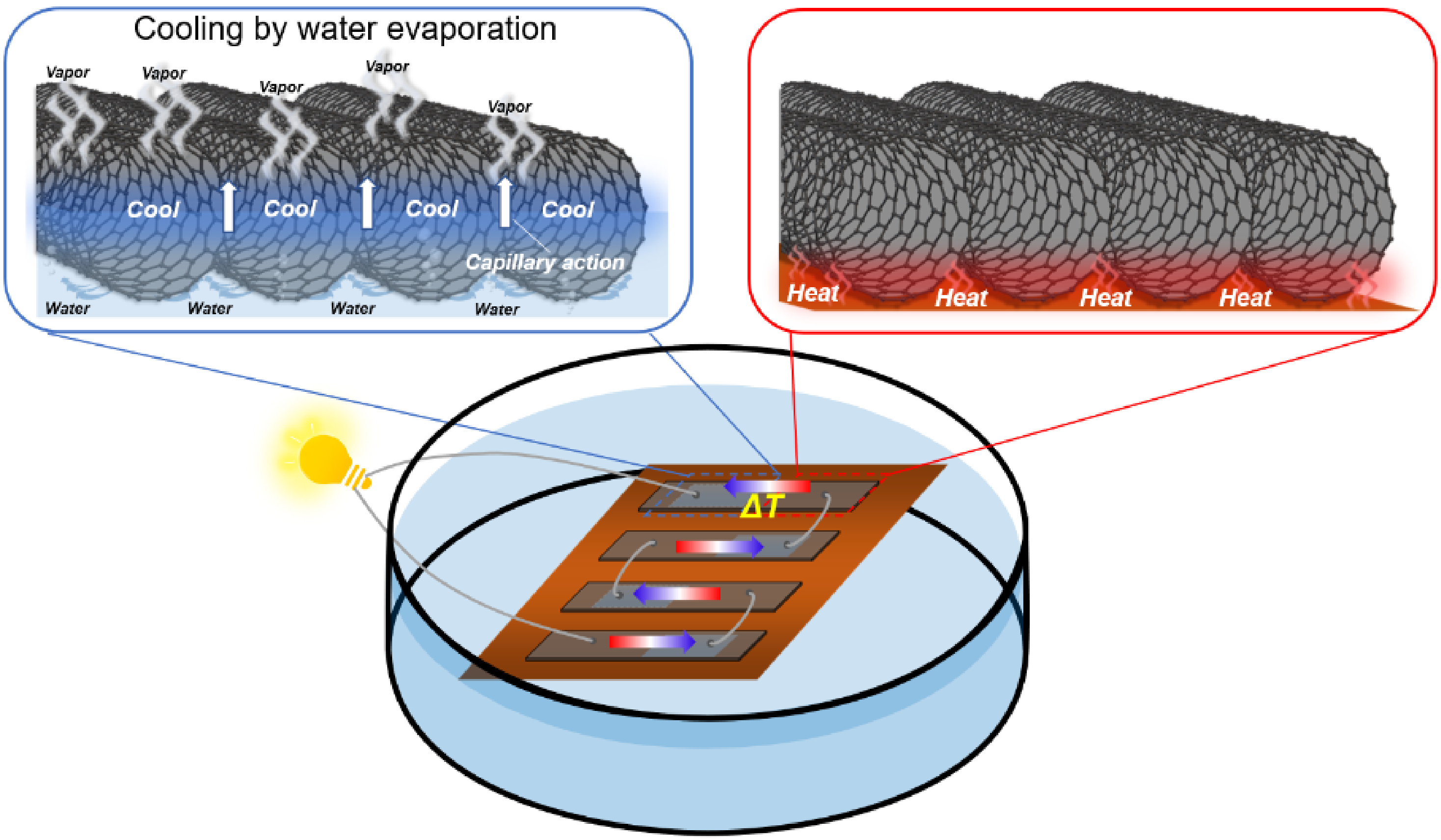

Figure 1

Design principle of water-floating SWCNT film TEGs. Each thin film is divided into water-permeable and water-nonpermeable areas. In the former, water passes through the gaps in the SWCNT bundle to reach the surface via capillary action. The surface temperature is reduced via an evaporation-induced cooling. Thus, a temperature gradient is created in each film, with thermoelectric power generated via the Seebeck effect.

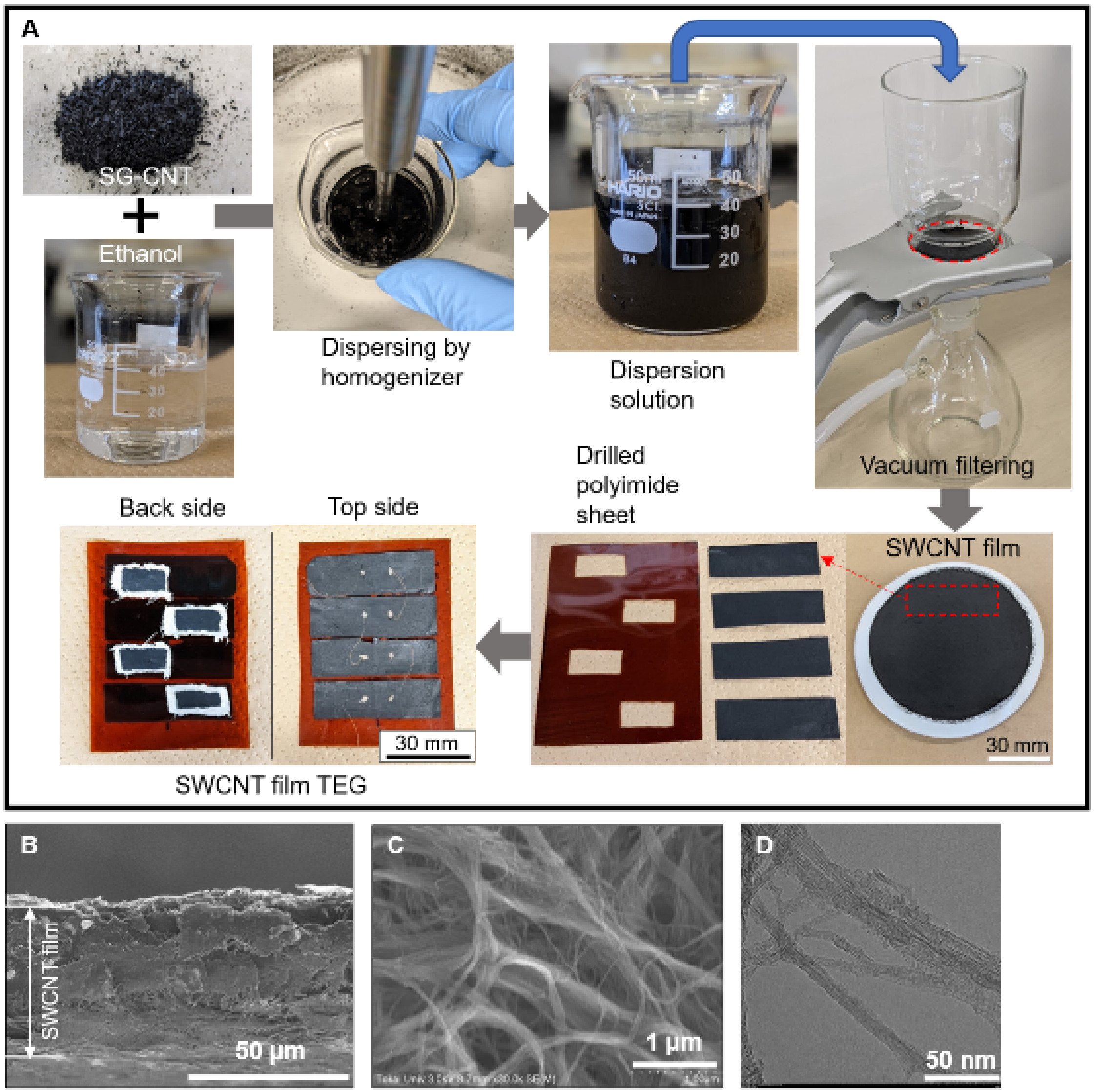

Figure 2

Fabrication and structural characterization of the water-floating SWCNT film TEGs. (a) Photographs showing the synthesis of SWCNT film TEGs. (b) SEM cross section of an SWCNT film. (c) SEM image of an SWCNT film surface. (d) TEM image of SWCNTs.

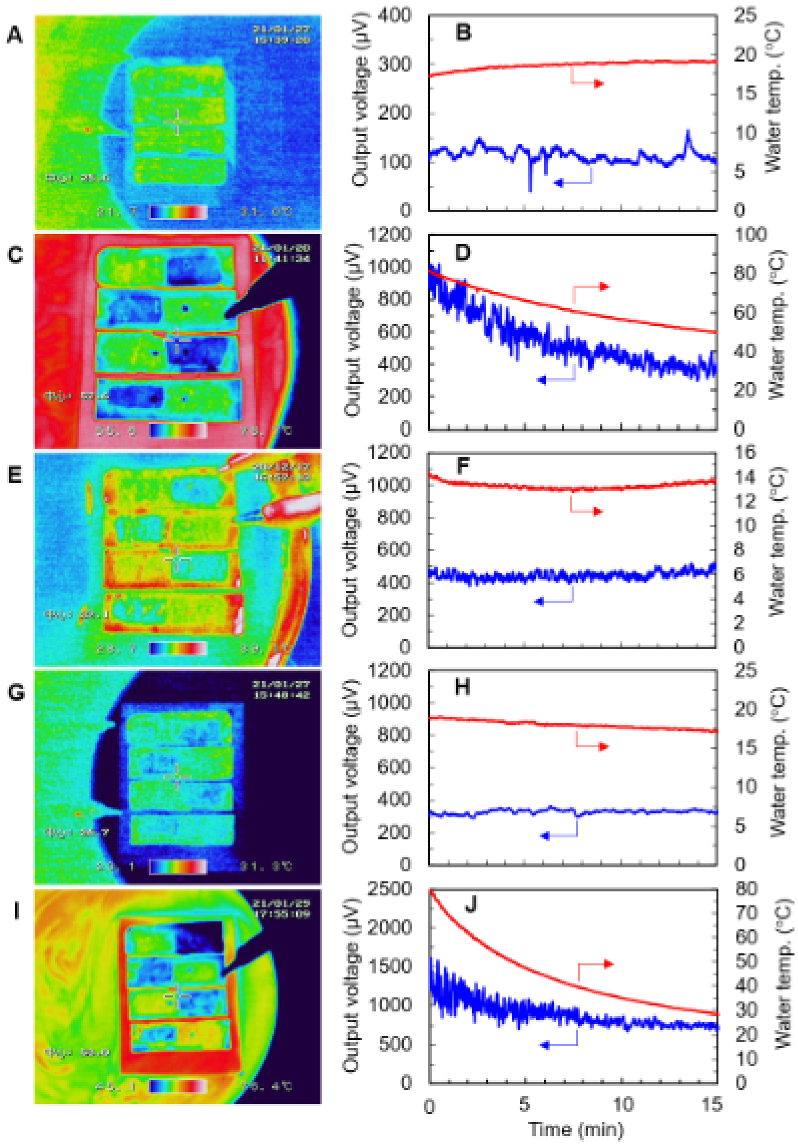

Figure 3

Temperature distribution and performance of the water-floating SWCNT film TEGs for various environmental conditions. Thermographic images of the TEG corresponding to (a) no sunlight or wind exposure at an initial temperature of approximately 20°C, (c) no sunlight or wind exposure at an initial temperature of approximately 80°C, (e) simulated sunlight but no wind, (g) wind but no simulated sunlight, and (i) both simulated sunlight and wind exposure at an initial temperature of approximately 80°C. (b), (d), (f), (h), and (j) Evolution of the output voltage (blue data) and water temperature (red data) corresponding to the conditions in (a), (c), (e), (g), and (i), respectively.

Supplementary Files

This is a list of supplementary files associated with this preprint. Click to download.

- 1404SuppleInfover6.docx